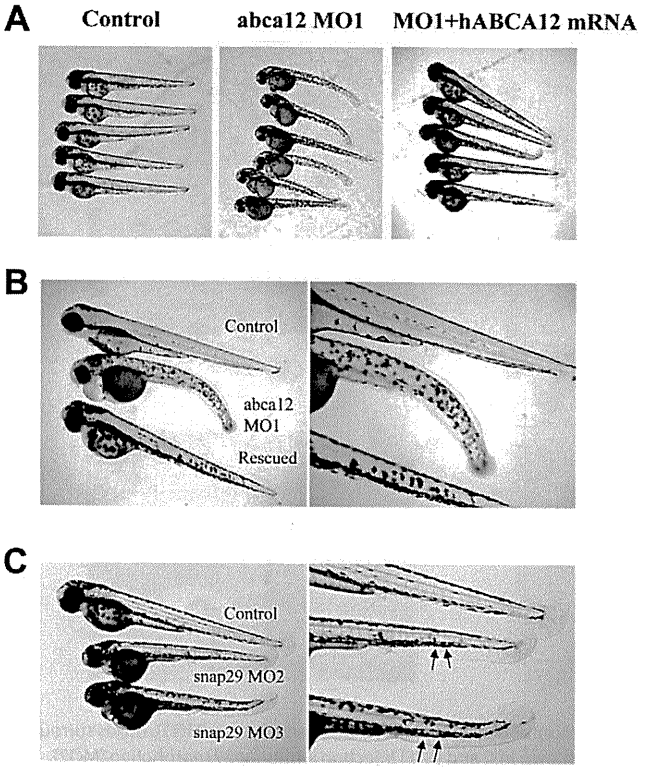

Fig. 4. Zebrafish phenotypes and their mRNA rescue at 3 dpf. (A) Phenotypic appearance of zebrafish larvae after injection with an *abca12* MO1 morpholino (middle panel) compared with control larvae (left panel), and partial rescue with human *ABCA12* mRNA (right panel). (B) Higher magnification of the larvae shown in A. (C) Phenotype of larvae at 3 dpf injected with *snap29* morpholinos MO2 or MO3. The irregular contour of the epidermis is noted by arrows.

pericardial edema. The rescue experiment, in addition to injection of control morpholinos, attested to the specificity of the phenotype documented in the morphant larvae. These experiments also confirmed that the zebrafish *abca12* gene is the functional homolog of human *ABCA12*.

Epidermal perturbations in zebrafish injected with *snap29* morpholino

Because knockdown of *abca12* expression was speculated to interfere with lipid secretion by lamellar granules, resulting in a characteristic epidermal phenotype, we proceeded to test this postulate by interfering with the lipid transport by another, independent mechanism: knockdown of the expression of the *snap29* gene. The corresponding protein, Snap29, has been suggested to mediate lipid transport within the epidermis and the deficiency of SNAP29 expression results in syndromic ichthyosis in patients with CEDNIK syndrome (Rapaport et al., 2010; Sprecher et al., 2005).

Surveying the zebrafish genome database revealed the presence of one *SNAP29*-related gene, *snap29*, on chromosome 8. This gene product had 52% identity with the human gene product at the protein level, and cladogram and syntenic analyses suggested that zebrafish *snap29* is the ortholog of human *SNAP29* (Fig. 1C). The expression of the gene was readily detectable at 2 dpf by RT-PCR and the expression level increased during 3-8 dpf (Fig. 2C). In situ hybridization of larvae showed weak, ubiquitous expression with accentuation of the labeling in the central nervous system marginal zone (not shown).

Injection of a morpholino (MO2) placed on the exon-4–intron-4 junction of the *snap29* gene into one- to four-cell-stage embryos inhibited the processing of pre-mRNA by >90% (Fig. 3B). A second, non-overlapping morpholino (MO3), placed on the intron-4–exon-5 border of the *snap29* gene similarly resulted in >90% inhibition of the splicing of intron 4 (data not shown). Examination of the morphant larvae at 3 dpf (n=165 for MO2, and n=203 for MO3) revealed a phenotype consisting of pigmentary changes, somewhat analogous with those noted with the *abca12* morpholino, in 80% of larvae, and the contour of the epidermis in the tail section was irregular (Fig. 4C). SEM of 20 morphant larvae revealed perturbations in the morphology of the epidermis that were very similar to those noted as a result of *abca12* knockdown (Fig. 5). Examination of the epidermis of the *snap29* morphant larvae (n=4) by TEM at 3 dpf revealed an increase in vesicles, which appeared empty under the same fixation conditions that revealed accumulation of lipid-like material in *abca12* morphant fish (Fig. 6E,F). Thus, interference by morpholino knockdown of the expression of two independent genes, *abca12* and *snap29*, that are involved in lipid transport in the epidermis can lead to similar phenotypic alterations in the epidermal morphology.

DISCUSSION

ABCA12 mutations underlie HI

The molecular basis of HI is linked to mutations in the *ABCA12* gene (Akiyama et al., 2005; Kelsell et al., 2005). Initial approaches utilizing single-nucleotide polymorphism-based chip technology and homozygosity mapping of families with individuals affected with HI placed the candidate gene locus on chromosomal region 2q35, and microsatellite markers narrowed the interval to consist of six genes (Kelsell et al., 2005). Several previous observations pointed to *ABCA12* as a candidate gene within the critical region. First, a characteristic ultrastructural feature of the epidermis in HI is an abnormality in the

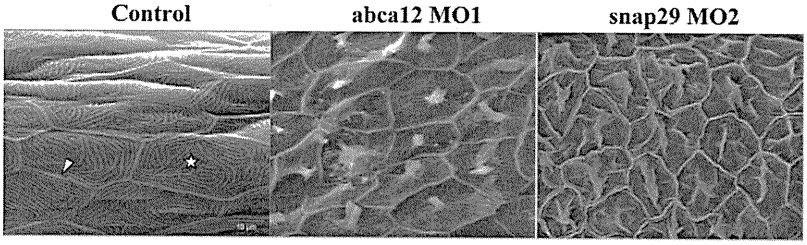

Fig. 5. SEM of the skin surface. The skin of the tail of the control larvae injected with the global standard control morpholino at 3 dpf shows the presence of keratinocytes with well-demarcated cell-cell borders (arrowhead) containing microridges (star; left panel). The morphant larvae injected with MO1 morpholino for *abca12* (middle) or *snap29* (MO2; right panel) revealed perturbed microridge formation with spicules in the center of the keratinocytes.

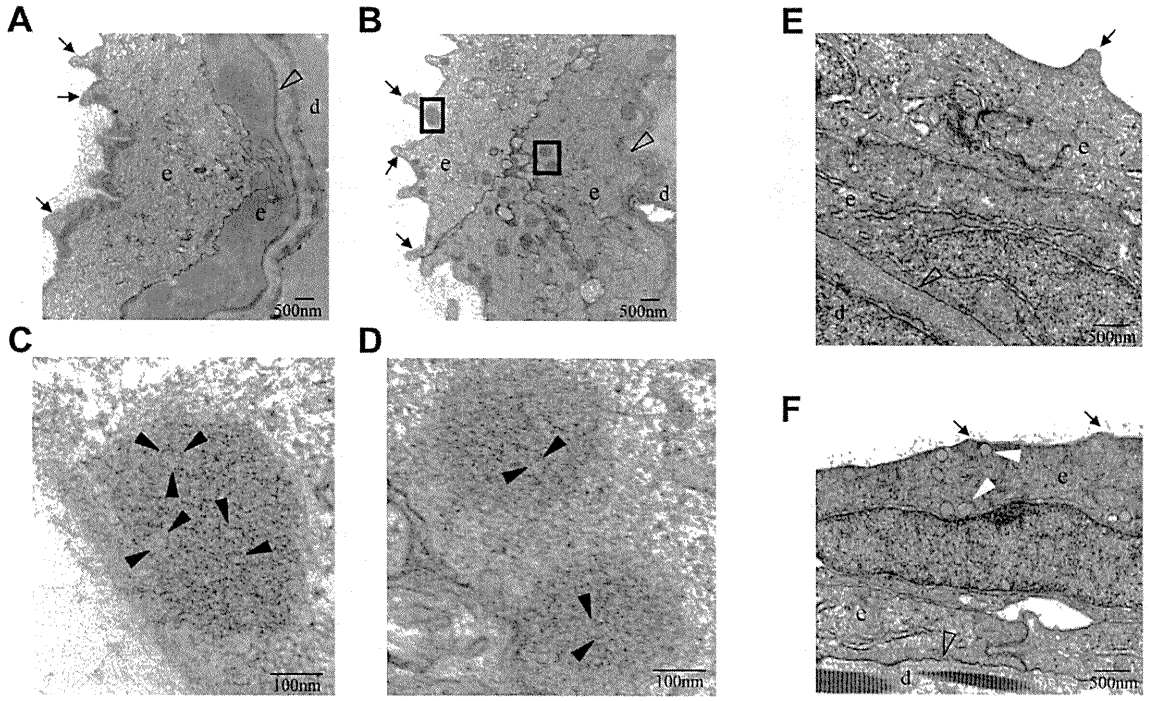

Fig. 6. TEM of 3-dpf larvae injected with *abca12* or *snap29* morpholinos. (A,E) Control morpholino (scMO); (B) *abca12* morpholino (MO1). Boxes surrounding electron-dense subcellular structures in B were examined at higher magnification and are shown in C and D. (F) Injection with *snap29* morpholino (MO2). (A-F) Arrows point to microridges; open arrowheads indicate basement membrane; solid black arrowheads point to the areas of accumulation of putative lipids within the electron-dense granules in C and D; solid white arrowheads in F point to apparently empty vesicles. e, epidermis; d, developing dermis.

localization of epidermal lipids, together with abnormal ultrastructural epidermal lamellar granules (Akiyama, 2006b). *ABCA12* has been suggested to encode a transmembrane transporter protein, which, from sequence homology with several other ABC family members, was thought to be involved in the transport of lipids (Kaminski et al., 2006). Second, the *ABCA12* gene was previously shown to harbor missense mutations in a milder form of ichthyosis, lamellar ichthyosis type 2 (LI2), with some resemblance to the phenotype in patients with HI who survive beyond the immediate postnatal period (Lefèvre et al., 2003). Currently, a total of 53 distinct mutations have been identified in the *ABCA12* gene (Akiyama, 2010).

Expression of *ABCA12* has been localized to lamellar granules. In normal epidermal keratinocytes there is an upregulation of *ABCA12* expression in association with physiological keratinization of the human epidermis (Sakai et al., 2007). Mutations in the *ABCA12* gene result in congested lipid retention in the skin of individuals with HI. It has been suggested that ABCA12 transports ceramides, the major lipid of the stratum corneum of the epidermis. Finally, lamellar-granule-mediated lipid secretion was resumed in the cultured keratinocytes of patients with HI upon transfer of the wild-type *ABCA12* gene (Akiyama et al., 2005). Thus, it is clear that mutations in the *ABCA12* transporter gene underlie HI.

abca12 and zebrafish skin development

In this study, we have demonstrated that zebrafish *abca12* is the ortholog of human *ABCA12*. There is a high degree of conservation of the Walker A and B motifs in addition to the retention of the four transmembrane domains containing one, five, one and five transmembrane segments, respectively. Zebrafish NBF1 and NBF2 domains in the Abca12 protein have 74% and 68% similarity with human NBF1 and NBF2 domains, respectively, at the amino acid level.

Whole-mount in situ hybridization in developing zebrafish embryos revealed that *abca12* was expressed in the EVL and the periderm. The EVL first appears at the 64-cell stage of development (~2 hpf) and is the outermost monolayer of cells surrounding the embryo. The EVL eventually gives rise to the periderm, which is thought to ultimately be replaced by the superficial stratum of the epidermis (Kimmel et al., 1995; Le Guellec et al., 2004). Although the physiology of zebrafish skin is still largely unexplored, the fact that *abca12* is expressed in the skin suggests its importance in normal skin development. This hypothesis is further strengthened by the results from our morpholino experiments. Injecting a morpholino that inhibited pre-mRNA splicing by >90% produced alterations in chromatophore distribution and the abnormal retention of lipids in both layers of the epidermis. Not only does this suggest that *abca12* is responsible for lipid transport in zebrafish, but the abnormal accumulation of lipids throughout the epidermis is a frequent finding in individuals with HI. Finally, the rescue of this phenotype by co-injection of human *ABCA12* mRNA shows that the phenotype is the result of *abca12* knockdown and not due to an off-target effect. In this context, it should be emphasized that the EVL-derived skin in zebrafish is embryologically different from the mammalian skin. Specifically, zebrafish epidermis does not undergo terminal differentiation, which in human skin culminates in the development of stratum corneum with barrier function. Emphasizing this

difference is the fact that survey of the current zebrafish genome database (Ensembl, Zebrafish Zv9; http://www.ensembl.org/Danio_rerio/Info/Index) does not reveal the presence of filaggrin, involucrin and trichohyalin genes, which are crucial for development of the stratum corneum in human epidermis (Li et al., 2011).

The role of lipids in epidermal development is further emphasized by our findings that knockdown of the expression of an independent gene, *snap29*, results in a similar epidermal phenotype as noted in *abca12* mutant larvae. Snap29 has been postulated to mediate lipid transport in the epidermis by facilitating membrane fusion of lamellar granules (Sprecher et al., 2005). Thus, interference of lipid trafficking by knockdown of two independent genes results in phenocopies of the epidermal perturbations in zebrafish, mimicking epidermal alterations in different forms of ichthyosis. It should be noted that, similar to the CEDNIK syndrome, ichthyosis has been reported in association with mental retardation, enteropathy, deafness, peripheral neuropathy and keratodermia, dubbed as the MEDNIK syndrome (Montpetit et al., 2008). This constellation was shown to be associated with a homozygous splice-site mutation in the *AP1S1* gene, encoding a subunit of the adaptor protein complex that regulates clathrin-coated vesicle assembly, protein cargo sorting, and vesicular trafficking between organelles in eukaryotic cells (Montpetit et al., 2008). The pathogenic effect of this mutation was validated by knockdown of *ap1s1* expression in zebrafish by a morpholino, resulting in perturbation in skin formation, reduced pigmentation and motility deficits. These findings, together with our observations in *snap29* mutant larvae, attest to the importance of vesicular trafficking in epidermal morphogenesis.

As indicated by morphological observations of the developing epidermis in zebrafish in comparison with human skin, there are clear differences. For example, the embryological origin of the EVL (periderm) in zebrafish is distinct from the basal layer in embryonic skin. In spite of this difference, there is an increasing body of evidence suggesting that the underlying molecular differentiation pathways are conserved between mammals and the zebrafish epidermis, based on molecular homologies (Sabel et al., 2009; Slanchev et al., 2009). Our work highlighting the early *abca12* expression in the EVL seems to support the conclusions that EVL forms the external layer of the embryonic and larval dermis and represents the initial differentiation of a true epidermis (Fukazawa et al., 2010).

Collectively, our results highlight the role of lipid transport and vesicular trafficking in epidermal development, and the results further suggest that zebrafish can serve as a model system to study different variants of ichthyosis, such as HI and the CEDNIK syndrome. Besides increasing our understanding of the disease mechanisms involved in ichthyotic syndromes, this model system is potentially useful for testing novel treatment modalities, for example by performing a small molecule library screen for compounds that are able to suppress the phenotype.

METHODS

Maintenance of zebrafish

Adult wild-type zebrafish were maintained under standard conditions at 28.5°C. Zebrafish embryos and larvae were also maintained at 28.5°C in a special embryo medium. All animals were housed in the zebrafish facility at Thomas Jefferson University and were cared for and used in accordance with University Institutional Animal Care and Use Committee guidelines and permission.

Phylogenetic and syntenic analyses

The genomic sequences of zebrafish were extracted from the Ensembl database. The zebrafish protein sequences were aligned with the corresponding proteins in different species by using ClustalW software (http://www.ebi.ac.uk/clustalw/).

The accession numbers for the *abca12* gene products in different species are: *E. caballus* (ENSECAP00000007797), *C. lupus familiaris* (XP_536058), *B. taurus* (XP_001788086), *H. sapiens* (NP_775099), *P. troglodytes* (XP_516070), *M. musculus* (XP_001002308), *R. norvegicus* (XP_237242), *G. gallus* (XP_421867), *D. rerio* (XP_686632) and *O. latipes* (ENSORLP00000020129). The accession numbers for *ABCC10* in *H. sapiens* is NP_258261. The accession numbers for *Abcc6* in different species are: *M. musculus* (NP_061265), *H. sapiens* (NP_001162), *D. rerio* (ENSDARP00000065432), *T. nigroviridis* (ENSTNIP00000015029) and *T. rubripes* (ENSTRUP00000029065).

The accession numbers for the *snap29* gene products in different species are: *H. sapiens* (NP_004773.1), *P. troglodytes* (XP_514997.2), *M. mulatta* (XP_001086227.1), *M. musculus* (NP_075837.3), *R. norvegicus* (NP_446262.3), *C. familiaris* (XP_543568.2), *B. taurus* (NP_001069427.1), *G. gallus* (NP_001025823.1), *D. rerio* (XP_700124.3), *S. salar* (NP_001134759.1), *X. laevis* (NP_001080076.1) and *A. thaliana* (NP_196405.1).

Phylogenetic analyses were conducted in the Molecular Evolution Genetics Analysis software (MEGA) version 4.0 (Tamura et al., 2007). The cladogram was constructed using the Neighbor-Joining method (Saitou and Nei, 1987). The Kimura two-parameter method was used to compute the evolutionary distances (Zuckerkandl and Pauling, 1965). The statistical reliance of NJ tree branches was evaluated using 1000 bootstrap samples.

For syntenic analysis, the orientation and chromosomal positions of *abca12* and *snap29* and their adjacent genes were determined manually from the gene orientations in the current Ensembl database. The zebrafish (Zv9), human (GRCh37/hg19), mouse (NCB137/mm9) and chicken (WUGSC2.1/galGal3) genome assembly versions were used for this analysis.

In situ hybridization

Whole-mount in situ hybridization was performed as described previously (Thisse and Thisse, 2008). Collected zebrafish embryos were fixed in 4% paraformaldehyde before hybridization. Digoxigenin (DIG)-labeled antisense and sense probes were synthesized. After hybridization, detection was performed with an anti-DIG antibody coupled to alkaline phosphatase.

Morpholinos and microinjection

Morpholino oligonucleotides were obtained from Gene Tools, LLC (Corvalis, OR). The morpholino oligomer sequences were written from 5′ to 3′, to correspond to the following genomic sequences (brackets surround the morpholino target sequence, exon sequences are capitalized, intron sequences are in lowercase, and nucleotide substitutions are bolded). For *abca12* knockdown: splice donor site morpholino (MO1), tgggaaataaatgtaatttacctgt, targets the exon-4–intron-4 junction, AAATGAAATAACTGA[ACAGgtaaattacatttatttccca]acggtc; 5-base pair mismatched control morpholino for *abca12* (cMO): tggc**a**aa**a**aaatct**a**atttac**g**tct. For *snap29* knockdown: splice donor site morpholino (MO2), ctgctcttgtgtttctcacccaggt, targets the exon-4–intron-4 junction,

GACAGAA[ACCTGGgtgagaaacacaagacag]cttctctcata; a second *snap29* splice junction morpholino (MO3) targets the intron 4-exon 5 border, ctcatctggaggacacaaacacaca, agtgtgtgtg[tgtgtg-tttgtgtcctccagATGAG]ATGTCTCTGGGTC. Global standard control morpholino (scMO), cctcttacctcagttacaatttata, has no target sequence in the zebrafish genome and is, therefore, inactive.

Embryos at the one- to four-cell stage were injected with an *abca12* morpholino (MO1, 25.6 ng) or *snap29* morpholinos (MO2, 2.6 ng and MO3, 5.2 ng) using glass microelectrodes fitted to a gas pressure injector (PL1-100, Harvard Apparatus). Electrodes were pulled (P-97, Flaming/Brown) and filled with morpholino and phenol red (final concentration 0.025%) to visualize the injected embryos. The embryos were then followed for viability, morphology and mRNA expression levels.

Total RNA isolation and cDNA synthesis

Zebrafish embryos were collected at 0 as well as 6 hpf and 1-8 dpf. They were disintegrated by pipetting through a 21 gauge needle and total RNA was extracted using TRIzol reagent (Invitrogen, Carlsbad, CA). To remove contaminating genomic DNA, RNase-free DNase I digestion (Fisher Scientific, St Louis, MO) was performed. 1 μg of total RNA was reverse transcribed using the Superscript III First-Strand cDNA synthesis kit (Invitrogen) according to the manufacturer's protocol. Controls were performed by omitting the reverse transcriptase enzyme. All cDNA samples were stored at −20°C for future use.

PCR amplification of cDNA

abca12 cDNA was amplified by PCR using a forward primer on exon 4 (5′-ATCTGGGACAACTTGGGCAACT-3′), and a reverse primer on exon 5 (5′-TCATCTGGTCAGCAGTTCCAGAGA-3′). The *snap29* cDNA was amplified using a forward primer on exon 4 (5′-TTCTGCTGCTCTTGATAACGGCT-3′), and a reverse primer on exon 5 (5′-TTTAAGGCTTTTGAGCTGCCGGTT-3′). Primers for the zebrafish *β-actin* gene (fwd: 5′-ATCTGGCACCACACCTTCTACAATG; rev: 5′-GGGGTG-TTGAAGGTCTCAAACATGAT) were used as a positive control. PCR was performed using Taq polymerase and Q buffer (Qiagen, Valencia, CA), according to the manufacturer's instructions. The PCR conditions were as follows: an initial denaturation at 94°C for 5 minutes, followed by 35 cycles of 94°C for 1 minute; 58°C for 1 minute; 72°C for 1 minute; and finally 72°C for 10 minutes. The intensity of the bands was quantified using ImageQuant version 5.0 software (Molecular Dynamics, Sunnyvale, CA).

mRNA rescue experiments

Capped full-length human mRNA corresponding to *ABCA12* was transcribed from an expression vector pCMV-Tag4B using the T3 mMessage mMachine kit (Ambion, Austin, TX). The morpholino was injected into one- to four-cell-stage embryos either alone or in combination with mRNA (2.3 ng) and followed for viability and morphology.

Scanning electron microscopy

Samples were fixed in neutral buffered formalin at room temperature for 2 hours, followed by a rinse with phosphate buffered saline and an ethanol dehydration series of exchanges by completely replacing each successively higher ethanol solution with the next higher (20, 30, 50, 75, 95 and 100%). Samples were then incubated for 15 minutes in a 1.5 ml micro test tube containing 1,1,2-Trichloro-1,2,2-trifluoroethane before covering the open micro test tube with parafilm, punching holes in it with a 30G needle, and situating it under a fume hood where it was dried by turbulent air flow. Samples were then mounted onto stubs with carbon paint and coated in 50 nm of gold using a sputter coater. Specimens were imaged in a JEOL-T330A scanning electron microscope (JEOL, Tokyo, Japan) at 15 kV.

TRANSLATIONAL IMPACT

Clinical issue

Ichthyosis comprises a group of cutaneous disorders characterized by dry, scaly skin and a broad spectrum of other phenotypic manifestations. One of the most severe forms of ichthyosis is known as harlequin ichthyosis (HI); neonates affected with HI are born encased in a thick skin that restricts their movement and frequently die shortly after birth. Some forms of ichthyosis are syndromic; for example, CEDNIK syndrome is so-named because it consists of cerebral dysgenesis, neuropathy, ichthyosis and keratoderma. Details of the pathomechanisms of HI have recently been revealed through molecular genetics, which showed that patients with this disorder carry mutations in the *ABCA12* gene. Examination of *Abca12*$^{-/-}$ mice suggested that this gene encodes a transmembrane transporter present in the epidermis that is postulated to transport lipids (specifically ceramides) and that is required for formation of the stratum corneum on the surface of the skin. Although the mouse model is useful in that it recapitulates features of human HI, drawbacks include the long gestational period and the small number of offspring produced per litter. CEDNIK syndrome is caused by mutations in the *SNAP29* gene, which is required for normal vesicle trafficking and lipid transport in the epidermis. There is no animal model for this syndrome.

Results

To create alternative, more expedient model systems to investigate pathological mechanisms of both HI and CEDNIK syndrome, the authors of this study knocked down the homologs of *ABCA12* and *SNAP29* in zebrafish embryos (*Danio rerio*). Morpholino antisense oligonucleotides targeted to exon-intron splice junctions were used to inhibit the splicing of *abca12* or *snap29* pre-mRNA. Inhibition of processing of either one of these mRNAs was accompanied by changes in the distribution of pigment along the trunk and tail of the fish as early as 2 days post-fertilization (dpf). Examination of epidermal morphology by scanning electron microscopy revealed perturbations in the surface contour of the keratinocytes, with loss of characteristic microridges and development of pathological spicules protruding from the center of each keratinocyte. These epidermal changes were accompanied by premature demise of the fish by 5 dpf. Transmission electron microscopy revealed an abundance of electron-dense granules in both morphants: lipid-like vesicles were seen in *abca12* knockdown fish, whereas the epidermis of *snap29* knockdown animals showed the presence of apparently empty vesicles.

Implications and future directions

This study demonstrates that inhibition of *abca12* or *snap29* gene splicing in zebrafish leads to epidermal perturbations that are similar to those seen in human patients with various forms of ichthyosis. In addition, it suggests that interfering with two independent pathways involved in lipid transport can result in phenotypically similar perturbations in epidermal morphogenesis. These systems can serve as models to study ichthyosis, and provide a means to develop pharmacological approaches towards treatment of this currently intractable group of diseases. Finally, in a broader sense, this study attests to the feasibility of using zebrafish as a model system to study heritable skin diseases.

Transmission electron microscopy

Samples were collected and fixed overnight at 4°C in 2.5% gluteraldehyde, 2% paraformaldehyde and 0.1 M sodium cacodylate. Samples were then washed in 0.1 M sodium cacodylate before undergoing secondary fixation in 2% osmium tetroxide, 1.5% potassium ferricyanide and 0.1 M sodium. Samples were again washed with 0.1 M sodium cacodylate followed by deionized water before undergoing en block staining with 2% uranyl acetate. Samples were washed again with deionized water, then dehydrated in a graded ethanol series and embedded in EMbed-812 (EMS, Hatfield, PA). Ultrathin sections (60 nm) were cut and analyzed using a JEOL JEM-1010 transmission electron microscope fitted with à Hamamatsu digital camera (Hamamatsu Photonics, Hamamatsu City, Japan) and AMT Advantage image capture software (AMT, Danvers, MA).

Statistical analysis

Risk differences and 95% confidence intervals were calculated between experimental groups with regards to survival, skin phenotype and edema in Table 1, for 3 dpf and 5 dpf separately. Fisher's exact test was used to determine the difference between proportions because of the presence of cells with zero observations. Adjustments for multiple comparisons were performed using False Discovery Rate, and it is these adjusted *P*-values that are reported. Analyses were conducted using SAS 9.2 (SAS Institute, Cary, NC).

ACKNOWLEDGEMENTS

The authors thank the following colleagues for advice and assistance: Wolfgang Driever, Institute for Biology I, University of Freiburg; Raymond Meade, Biomedical Imaging Core Facility, University of Pennsylvania; Gerald Harrison, Department of Biochemistry, School of Dental Medicine, University of Pennsylvania; Jean-Yves Sire, Equipe "Evolution et Développement du Squelette", Université Paris; Eijiro Adachi, Department of Matrix Biology and Tissue Regeneration, Graduate School of Medical Sciences, Kitasato University; Ulrich Rodeck, Gabor Kari, April Aguillard, Adele Donahue and Andrzej Fertala, Department of Dermatology and Cutaneous Biology, Thomas Jefferson University; Terry Hyslop and Jocelyn Andrel, Department of Pharmacology and Experimental Therapeutics, Thomas Jefferson University. Carol Kelly assisted in manuscript preparation. This study was supported by the NIH/NIAMS grant R01AR055225 to J.U.; by the University of Virginia to C.T. and B.T. Q.L. is a recipient of a Research Career Development Award from the Dermatology Foundation.

COMPETING INTERESTS

The authors declare that they do not have any competing or financial interests.

AUTHOR CONTRIBUTIONS

Q.L., M.F., C.T. and B.T. performed the experiments; M.A. provided reagents; H.S. and E.S. interpreted the data and edited the manuscript; S.-Y.H. contributed to the data analysis; J.U. developed the concept, interpreted the data and prepared the manuscript.

REFERENCES

Akiyama, M. (2006a). Harlequin ichthyosis and other autosomal recessive congenital ichthyoses: the underlying genetic defects and pathomechanisms. *J. Dermatol. Sci.* **42**, 83-89.

Akiyama, M. (2006b). Pathomechanisms of harlequin ichthyosis and ABCA transporters in human diseases. *Arch. Dermatol.* **142**, 914-918.

Akiyama, M. (2010). *ABCA12* mutations in harlequin ichthyosis, congenital ichthyosiform erythroderma and lamellar ichthyosis. *Hum. Mutat.* **31**, 1090-1096.

Akiyama, M., Sugiyama-Nakagiri, Y., Sakai, K., McMillan, J. R., Goto, M., Arita, K., Tsuji-Abe, Y., Tabata, N., Matsuoka, K. and Sasaki, R. (2005). Mutations in lipid transporter ABCA12 in harlequin ichthyosis and functional recovery by corrective gene transfer. *J. Clin. Invest.* **115**, 1777-1784.

Brown, S. J. and Irvine, A. D. (2008). Atopic eczema and the filaggrin story. *Semin. Cutan. Med. Surg.* **27**, 128-137.

Brown, S. J. and McLean, W. H. I. (2008). Eczema genetics: current state of knowledge and future goals. *J. Invest. Dermatol.* **129**, 543-552.

Elias, P. M., Crumrine, D., Rassner, U., Hachem, J. P., Menon, G. K., Man, W., Choy, M. H., Leypoldt, L., Feingold, K. R. and Williams, M. L. (2004). Basis for abnormal desquamation and permeability barrier dysfunction in RXLI. *J. Invest. Dermatol.* **122**, 314-319.

Fuchs-Telem, D., Stewart, H., Rapaport, D., Nousbeck, J., Gat, A., Gini, M., Lugassy, Y., Emmert, S., Eckl, K., Hennies, H. C. et al. (2011). CEDNIK syndrome results from loss-of-function mutations in SNAP29. *Br. J. Dermatol.* **164**, 610-616.

Fukazawa, C., Santiago, C., Park, K. M., Deery, W. J., Gomez de la Torre Canny, S., Holterhoff, C. K. and Wagner, D. A. (2010). poly/chuk/ikk1 is required for differentiation of the zebrafish embryonic epidermis. *Dev. Biol.* **346**, 272-283.

Kaminski, W. E., Piehler, A. and Wenzel, J. J. (2006). ABC A-subfamily transporters: structure, function and disease. *Biochim. Biophys. Acta* **1762**, 510-524.

Kari, G., Rodeck, U. and Dicker, A. P. (2007). Zebrafish: an emerging model system for human disease and drug discovery. *Clin. Pharmacol. Ther.* **82**, 70-80.

Kelsell, D. P., Norgett, E. E., Unsworth, H., Teh, M. T., Cullup, T., Mein, C. A., Dopping-Hepenstal, P. J., Dale, B. A., Tadini, G. and Fleckman, P. (2005). Mutations in ABCA12 underlie the severe congenital skin diseases harlequin ichthyosis. *Am. J. Hum. Genet.* **76**, 794-803.

Kimmel, C. B., Ballard, W. W., Kimmel, S. R., Ullmann, B. and Schilling, T. F. (1995). Stages of embryonic development of the zebrafish. *Dev. Dyn.* **203**, 253-310.

Le Guellec, D., Morvan-Dubois, G. and Sire, J. Y. (2004). Skin development in bony fish with particular emphasis on collagen deposition in the dermis of the zebrafish (Danio rerio). *Int. J. Dev. Biol.* **48**, 217-232.

Lefèvre, C., Audebert, S., Jobard, F., Bouadjar, B., Lakhdar, H., Boughdene-Stambouli, O., Blanchet-Bardon, C., Heilig, R., Foglio, M. and Weissenbach, J. (2003). Mutations in the transporter ABCA12 are associated with lamellar ichthyosis type 2. *Hum. Mol. Genet.* **12**, 2369-2378.

Li, Q., Frank, M., Thisse, C., Thisse, B. and Uitto, J. (2011). Zebrafish: a model system to study heritable skin diseases. *J. Invest. Dermatol.* **131**, 565-571.

McGrath, J. A. and Uitto, J. (2008). The filaggrin story: novel insights into skin-barrier function and disease. *Trends Mol. Med.* **14**, 20-27.

Montpetit, A., Côté, S., Brustein, E., Drouin, C. A., Lapointe, L., Boudreau, M., Meloche, C., Drouin, R., Hudson, T. J., Drapeau, P. et al. (2008). Disruption of AP1S1, causing a novel neurocutaneous syndrome, perturbs development of the skin and spinal cord. *PloS Genet.* **4**, e1000296.

Rapaport, D., Lugassy, Y., Sprecher, E. and Horowitz, M. (2010). Loss of SNAP29 impairs endocytic recycling and cell motility. *PloS ONE* **5**, e9759.

Sabel, J. L., d'Alençon, C., O'Brien, E. K., Van Otterloo, E., Lutz, K., Cuykendall, T. N., Schutte, B. C., Houston, D. W. and Cornell, R. A. (2009). Maternal interferon regulatory factor 6 is required for the differentiation of primary superficial epithelia in Danio and Xenopus embryos. *Dev. Biol.* **325**, 249-263.

Saitou, N. and Nei, M. (1987). The neighbor-joining method: a new method for reconstructing phylogenetic trees. *Mol. Biol. Evol.* **4**, 406-425.

Sakai, K., Akiyama, M., Sugiyama-Nakagiri, Y., McMillan, J. R., Sawamura, D. and Shimizu, H. (2007). Localization of ABCA12 from golgi apparatus to lamellar granules in human upper epidermal keratinocytes. *Exp. Dermatol.* **16**, 920-926.

Slanchev, K., Carney, T. J., Stemmler, M. P., Koschorz, B., Amsterdam, A., Schwarz, H. and Hammerschmidt, M. (2009). The epithelial cell adhesion molecule EpCAM is required for epithelial morphogenesis and integrity during zebrafish epiboly and skin development. *PLoS Genet.* **5**, e1000563.

Smyth, I., Hacking, D. F., Hilton, A. A., Mukhamedova, N., Meikle, P. J., Ellis, S., Satterley, K., Collinge, J. E., de Graaf, C. A. and Bahlo, M. (2008). A mouse model of harlequin ichthyosis delineates a key role for Abca12 in lipid homeostasis. *PLoS Genet.* **4**, e1000192.

Sprecher, E., Ishida-Yamamoto, A., Mizrahi-Koren, M., Rapaport, D., Goldsher, D., Indelman, M., Topaz, O., Chefetz, I., Keren, H., O'Brien, T. J. et al. (2005). A mutation in SNAP29, coding for a SNARE protein involved in intracellular trafficking, causes a novel neurocutaneous syndrome characterized by cerebral dysgenesis, neuropathy, ichthyosis, and palmoplantar keratoderma. *Am. J. Hum. Genet.* **77**, 242-251.

Sundberg, J. P., Boggess, D., Hogan, M. E., Sundberg, B. A., Rourk, M. H., Harris, B., Johnson, K., Dunstan, R. W. and Davisson, M. T. (1997). Harlequin ichthyosis (ichq): a juvenile lethal mouse mutation with ichthyosiform dermatitis. *Am. J. Pathol.* **151**, 293-310.

Tamura, K., Dudley, J., Nei, M. and Kumar, S. (2007). MEGA4: molecular evolutionary genetics analysis (MEGA) software version 4.0. *Mol. Biol. Evol.* **24**, 1596-1599.

Thisse, C. and Thisse, B. (2008). High resolution in situ hybridization on whole-mount zebrafish embryo. *Nat. Protoc.* **3**, 59-69.

Tusnády, G. E., Sarkadi, B., Simon, I. and Váradi, A. (2006). Membrane topology of human ABC proteins. *FEBS Lett.* **580**, 1017-1022.

Yanagi, T., Akiyama, M., Nishihara, H., Sakai, K., Nishie, W., Tanaka, S. and Shimizu, H. (2008). Harlequin ichthyosis model mouse reveals alveolar collapse and severe fetal skin barrier defects. *Hum. Mol. Genet.* **17**, 3075-3083.

Zuckerkandl, E. and Pauling, L. (1965). Evolutionary divergence and convergence in proteins. In *Evolving Genes and Proteins* (ed. V. Bryson and H. J. Vogel), pp. 97-166. New York: Academic Press.

thickness of the mucous layer of small intestines, resulting in the inhibition of small intestinal absorption.[4] In addition, PGE1 increases blood flow in the stomach and upregulates the digestion in the stomach. During the provocation test in our case, serum gliadin levels were not increased by administering misoprostol. However, sodium cromoglicate, a mast cell stabilizer commonly used to treat allergic rhinitis, allergic conjunctivitis, and asthma, could not affect serum gliadin levels in the provocation test, and therefore allowed the symptoms to occur. We consider that the effects of misoprostol on the alimentary tract are crucial for the prevention of FDEIA. Our observation indicates that the exacerbating effect of aspirin in FDEIA comes from the inhibitory effects of aspirin on PGE1 in the gastrointestinal milieu. Thus, misoprostol would be a promising prophylactic drug for FDEIA.

Aya Takahashi, MD
Kimiko Nakajima, MD
Mitsunori Ikeda, MD
Shigetoshi Sano, MD
Department of Dermatology
Kochi Medical School, Nankoku
Kochi
Japan

Kunie Kohno, MD
Eishin Morita, MD
Department of Dermatology
Shimane University Faculty of Medicine
Izumo, Shimane
Japan
E-mail: jm-aya.derm@kochi-u.ac.jp

References

1 Matsuo H, Morita E, Tatham AS, *et al.* Identification of the IgE-binding epitope in omega-5 gliadin, a major allergen in wheat-dependent exercise-induced anaphylaxis. *J Biol Chem* 2004; 279: 12135–40.
2 Matsuo H, Morimoto K, Akaki T, *et al.* Exercise and aspirin increase levels of circulating gliadin peptides in patients with wheat-dependent exercise-induced anaphylaxis. *Clin Exp Allergy* 2005; 35: 461–6.
3 Sheffer AL, Tong AK, Murphy GF, *et al.* Exercise-induced anaphylaxis: a serious form of physical allergy associated with mast cell degranulation. *J Allergy Clin Immunol* 1985; 75: 479–84.
4 Gurleyik E, Coskun O, Ustundag N, *et al.* Prostaglandin E1 maintains structural integrity of intestinal mucosa and prevents bacterial translocation during experimental obstructive jaundice. *J Invest Surg* 2006; 19: 283–9.

Type XVII collagen ELISA indices significantly decreased after bullous pemphigoid remission

The major pathogenic epitope of bullous pemphigoid (BP) is known to be the noncollagenous extracellular domain (NC16A) of type XVII collagen (COL17).[1] Here we investigated indirect immunofluorescence (IIF) and COL17 NC16A domain enzyme-linked immunosorbent assay (ELISA)[2–5] data before treatment and after remission to evaluate the usefulness of ELISA analyses as indicators for BP disease activity.

We included ten consecutive BP patients [eight women and two men: between 33 and 80 years old (mean; 59 years old)] who showed typical clinical features before treatment and were successfully treated, resulting in complete or partial remission at our institute. The first day of each patient visit was within the last three years. In all patients, the diagnosis was confirmed by histopathological observation and immunofluorescence study, i.e. histopathological subepidermal blister formation was observed and direct and IIF studies revealed the presence of autoantibodies along the dermal–epidermal junction. All patients were successfully treated with oral prednisolone therapy of 30–50 mg/d with or without azathioprine or a combination therapy using tetracycline and nicotinamide. Treatment periods from initial diagnosis to remission ranged from four months to 35 months (mean; 14.6 ± 10.8 months). Serum samples were obtained for ELISA and IIF at least twice during the disease course for each patient.

Concentration of autoantibodies in the patients' sera directed against the NC16A domain of COL17 was measured using the COL17 NC16A ELISA kit following the kit's instructions.[6] IIF staining and evaluation were performed as previously described using normal human skin as a substrate.[7]

In all the cases, the ELISA indices showed a decrease during the successful treatment course. ELISA indices after remission were significantly reduced compared with those before treatment ($P < 0.0001$) (Fig. 1a). IIF titers also decreased after remission in six cases, but the titers were not apparently reduced in the other four cases, although a statistically significant reduction in combined IIF titer was observed after remission compared with those before treatment ($P < 0.05$) (Fig. 1b).

Positive correlation between ELISA indices and BP disease activity has been reported previously in the literature. Di Zenzo *et al.*[8] demonstrated that disease severity before treatment was well correlated with ELISA indices in BP patients. Izumi *et al.*[9] described ELISA indices and alteration of disease activity of five BP patients during various treatments. In this study, we compared the ELISA

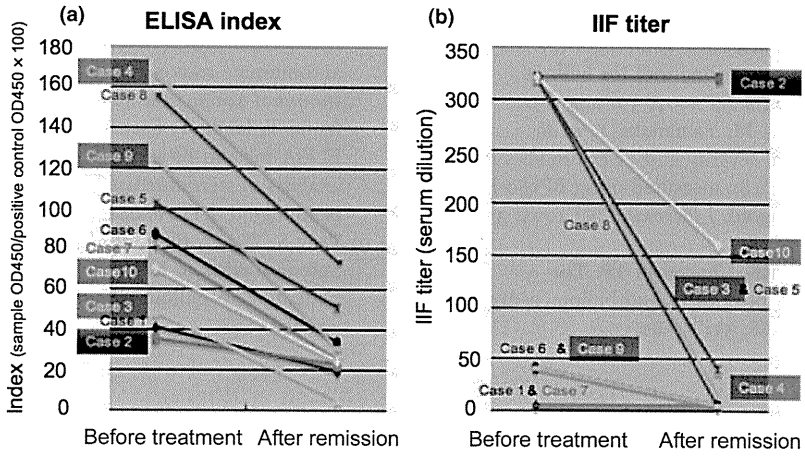

Figure 1 ELISA indices and indirect immunofluorescence (IIF) titers before treatment and after remission. (a) ELISA indices of successfully treated BP patients. Disease remission was defined as when erythema, bullae and erosions had completely healed (complete remission) or no more than three bullae or erythema were seen in a week (partial remission) and only a low dose of oral prednisolone (<5 mg/d) or no treatment was needed to maintain this condition. As ELISA indices after remission, we adopted ELISA indices at the time when each patient's disease activity was evaluated as being in "complete remission" or "partial remission" (as defined above) for the first time after treatment. Mean ELISA index of the 10 patients before treatment was 91.3 ± 45.7 (range: 35.6–165.6) and the mean index after remission was 37.4 ± 25.3 (range: 6.0–86.4). After complete or partial remission, the ELISA indices were significantly reduced ($P < 0.0001$). (b) IIF titers of the same patients. Apparent decreases in IIF titers after remission were seen only in six patients. Mean IIF titer of the 10 patients before treatment was 201 ± 154 (range: 5–320) and the mean titer after remission was 60.5 ± 102.8 (range: 5–320). A statistically, significant reduction was observed in combined IIF titers after remission compared with those before treatment ($P < 0.05$). Colors of the lines are specific for each patient in both figures (a) and (b)

indices before treatment and after remission in our BP patient cohort and clearly demonstrated that ELISA indices significantly decreased after remission. Feng *et al.*[10] reported similar results on correlation of ELISA indices with disease course in BP patients, although the time points for ELISA after treatment were just before the decrease in corticosteroid and when the dosage of corticosteroid was successfully decreased to half the initial dose in the report. In this study, we employed ELISA indices at the time when each patient's disease activity was evaluated as "complete remission" or "partial remission" for the first time after treatment. Thus, this study is unique in the point that we evaluated exact correlation between ELISA indices and disease remission.

In conclusion, the present results further support the idea that the COL17 NC16A ELISA indices demonstrate a correlation with the BP disease remission more accurately than IIF titers and are a useful tool to detect BP disease remission and to assess the efficacy of BP treatment.

Erika Kusajima
Masashi Akiyama, MD, PhD
Megumi Sato
Ken Natsuga, MD
Hiroshi Shimizu, MD, PhD
Department of Dermatology
Hokkaido University Graduate School of Medicine
Sapporo
Japan
E-mail: akiyama@med.hokudai.ac.jp
Conflict of interest: the authors state no conflict of interest.

References

1 Giudice GJ, Emery DJ, Zelickson BD, *et al.* Bullous pemphigoid and herpes gestationis autoantibodies recognize a common non-collagenous site on the BP180 ectodomain. *J Immunol* 1993; 151: 5742–5750.
2 Zillikens D, Mascaro JM, Rose PA, *et al.* A highly sensitive enzyme-linked immunosorbent assay for the detection of circulating anti-BP180 autoantibodies in patients with bullous pemphigoid. *J Invest Dermatol* 1997; 109: 679–683.
3 Hata Y, Fujii Y, Tsunoda K, Amagai M. Production of the entire extracellular domain of BP180 (type XVII collagen) by baculovirus expression. *J Dermatol Sci* 2000; 23: 183–190.
4 Schmidt E, Obe K, Brocher EB, Zillikens D. Serum levels of autoantibodies to BP180 correlate with disease activity in patients with bullous pemphigoid. *Arch Dermatol* 2000; 136: 174–178.

5 Kobayashi M, Amagai M, Kuroda-Kinoshita K, *et al.* BP180 ELISA using bacterial recombinant NC16a protein as a diagnostic and monitoring tool for bullous pemphigoid. *J Deramtol Sci* 2002; 30: 224–232.
6 Tsuji-Abe Y, Akiyama M, Yamanaka Y, *et al.* Correlation of clinical severity and ELISA indices for the NC16A domain of BP180 measured using BP180 ELISA kit in bullous pemphigoid. *J Dermatol Sci* 2005; 37: 145–149.
7 Beutner EH, Jordon RE, Chorzelski TP. The immunopathology of pemphigus and bullous pemphigoid. *J Invest Dermatol* 1968; 51: 63–80.
8 Di Zenzo G, Thoma-Uszynski S, Fontao L, *et al.* Multicenter prospective study of the humoral autoimmune response in bullous pemphigoid. *Clin Immunol* 2008; 128: 415–426.
9 Izumi T, Ichiki Y, Esaki C, Kitajima Y. Monitoring of ELISA for anti-BP180 antibodies: clinical and therapeutic analysis of steroid-treated patients with bullous pemphigoid. *J Dermatol* 2004; 31: 383–391.
10 Feng S, Wu Q, Jin P, *et al.* Serum levels of autoantibodies to BP180 correlate with disease activity in patients with bullous pemphigoid. *Int J Dermatol* 2008; 47: 225–228.

prednisolone in HIV-infected individuals. J Acquir Immune Defic Syndr 2008;48:561-6.
5. Dort K, Padia S, Wispelwey B, Moore CC. Adrenal suppression due to an interaction between ritonavir and injected triamcinolone: a case report. AIDS Res Ther 2009;6:10.

doi:10.1016/j.jaad.2010.09.014

Subepidermal blistering disease with 3 distinct autoantibodies: Anti-BP230, anti-laminin gamma-1, and anti-laminin-332

To the Editor: A 25-year-old Japanese woman presented with pruritic tense blisters involving the lips, forearms, fingers, and soles (Fig 1, *A-C*). No mucosal involvement was observed. A skin biopsy specimen taken from a bulla on her left forearm demonstrated subepidermal separation with eosinophilic inflammatory infiltrate in the dermis (Fig 2, *A*). Direct immunofluorescence (IF) microscopy of the lesion showed linear deposition of C3 and IgG at the dermoepidermal junction (Fig 2, *B* and *C*). Indirect IF on sodium-split skin revealed linear IgG deposition on both the epidermal and the dermal sides (titer 1:20; Fig 2, *D*). Enzyme-linked immunosorbent assay (ELISA) using bacterial recombinant protein of the NC16a domain of COL17 (MBL, Nagoya, Japan) was negative. ELISA using bacterial recombinant proteins of the N- and C-terminal domains of BP230 (MBL, Nagoya, Japan) was also negative. Immunoblot analysis with epidermal and dermal extracts derived from normal human skin and purified laminin-332 was performed. The results showed the presence of circulating IgG autoantibodies against BP230, laminin γ1, and the γ 2 chain of laminin-332 (Fig 2, *E*, *F*, and *G*). Oral prednisolone, 40 mg per day (PSL), failed to alleviate the symptoms. With the addition of 75 mg per day of oral diaphenylsulfone (DDS), the cutaneous lesions rapidly healed with postinflammatory hyperpigmentation. PSL and DDS were tapered without relapse of skin lesions. At 10 months after referral, she discontinued PSL and was taking DDS at 25 mg daily.

Previously, antibodies against laminin-332 were detected in about 10% to 20% of mucous membrane pemphigoid (MMP) patients. The majority of the patients have antibodies reactive with the α3 subunit of the protein. However, our case showed reactivity only with the γ2 subunit. The mucosal involvement that is typically seen in MMP was not observed in our case.

Circulating antibodies against BP230 were detected in the serum of a patient by immunoblot analysis but not by BP230 ELISA (MBL, Nagoya, Japan). This ELISA system utilizes the N- and C-terminal domains of BP230, but not the central-rod domain.[1] Therefore the autoantibodies against BP230 that were detected in our immunoblot study may have reacted with the central-rod domain of the BP230 antigen. Autoantibodies against BP230, an intracellular protein, are clearly associated with bullous pemphigoid (BP), but have not been shown to be involved in the initiation of the disease. A marked improvement with the administration of DDS and the absence of erythematous plaques in the patient were not typical of the BP clinical course and manifestations.

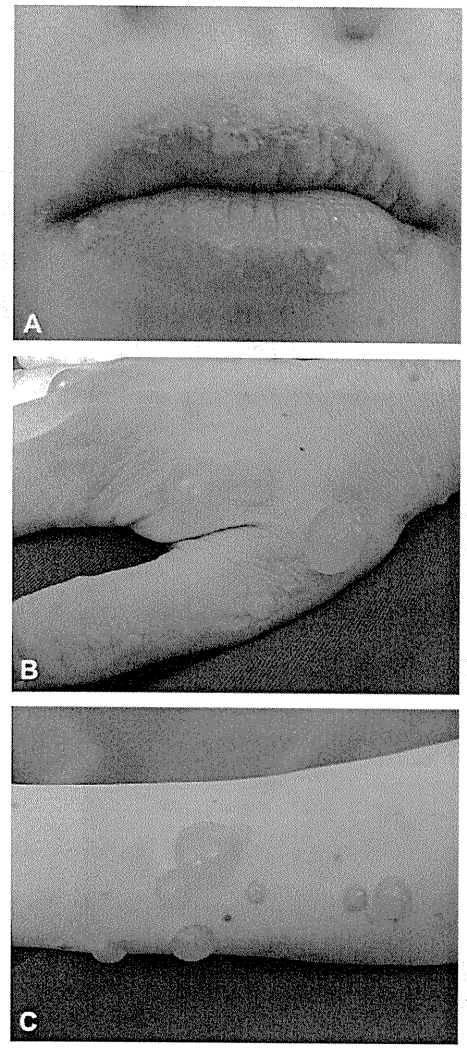

Fig 1. Clinical presentation of the patient. Tense blisters involve the fingers (**A**), forearms (**B**), and lips (**C**).

Autoantibodies against laminin γ1 are characteristic of anti-laminin γ1 pemphigoid.[2] Blisters involving the lips and therapeutic improvement with DDS are compatible with the clinical features of anti-laminin γ1 pemphigoid. On the basis of these findings, the diagnosis of anti-laminin γ1 pemphigoid may be appropriate.

It is possible that the unusual autoimmune profile of the patient developed as a result of epitope

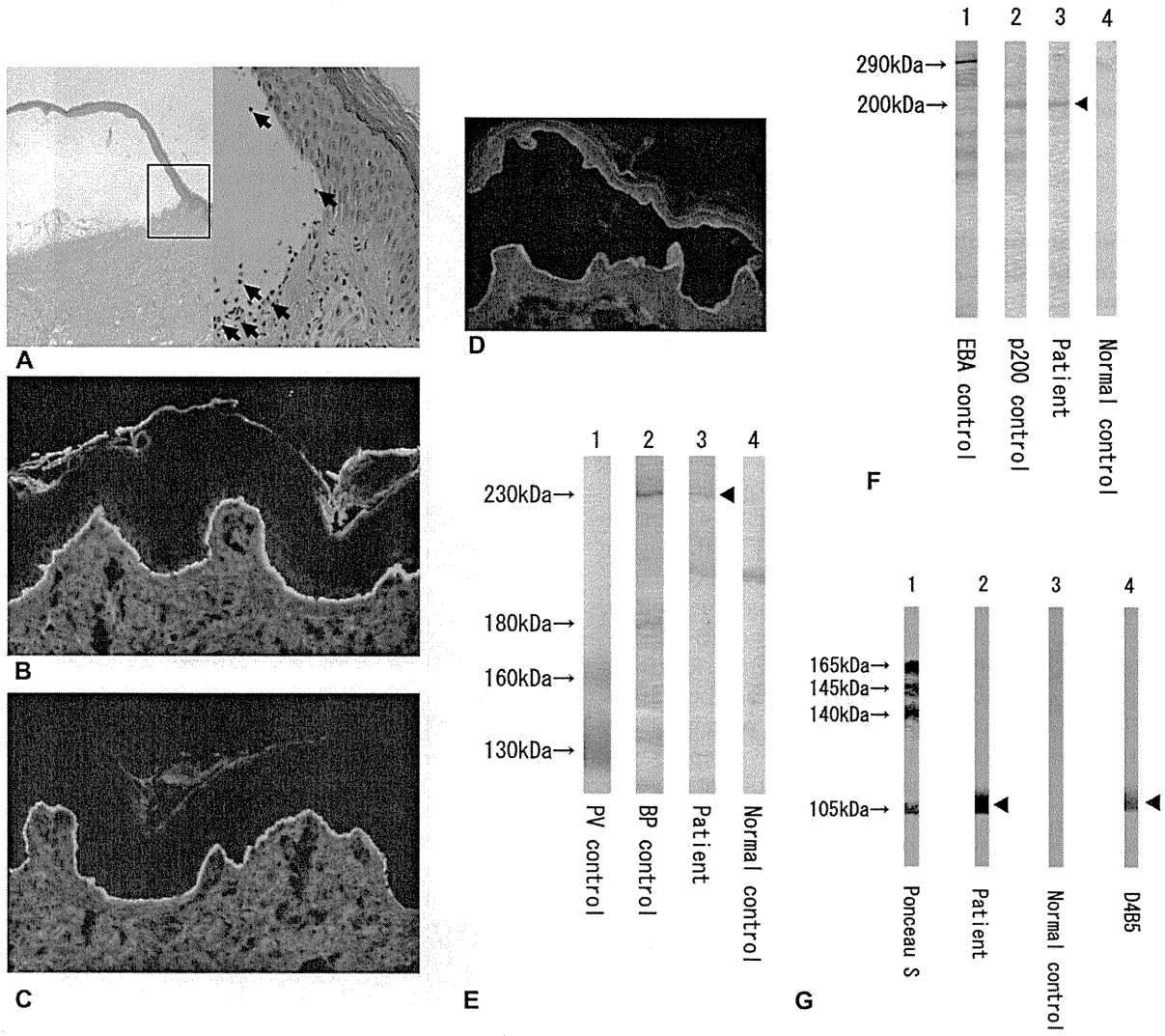

Fig 2. Histologic examination of skin specimens from patient's left forearm. **A**, Hematoxylin-eosin stain. Subepidermal blister (original magnification: ×40) with infiltration of eosinophils (*arrows*) in blister cavity (×200). Direct immunofluorescence of perilesional skin samples shows linear deposition of C3 (**B**) and IgG (**C**) at the dermoepidermal junction (×40). Immunological characterization of autoantibodies. **D**, Indirect immunofluorescence on 1M NaCl-split skin. Circulating IgG antibodies bind to both epidermal and dermal sides (titer 1:20). **E**, Immunoblot analysis using human epidermal extracts. *Lane 1*: A reference BP serum reacting with 180-kd (COL17) and 230-kd (BP230) antigens. *Lane 2*: A reference pemphigus vulgaris serum with positive bands at 130 kd (Dsg3) and 160 kd (Dsg1). *Lane 3*: Patient's serum. IgG in patient's serum reacts with BP230. **F**, Immunoblot analysis using human dermal extracts. *Lane 1*: A reference EBA serum reacting with a 290-kd molecule (type VII collagen). *Lane 2*: A reference anti-laminin γ1 pemphigoid serum with a positive band at 200 kd (p200, laminin γ1). *Lane 3*: Patient's serum. *Lane 4*: A reference normal serum. IgG in patient's serum reacts with 200-kd antigen. **G**, Immunoblot analysis using purified laminin-332 (courtesy of Dr S. Amano, Shiseido Life Science Research Center, Yokohama, Japan). *Lane 1*: A reference of Ponceau S stain of laminin-332 consisting of α3 (165 kd, 145 kd), β3 (140 kd), and γ2 (105 kd) subunits. *Lane 2*: Patient's serum. *Lane 3*: A reference normal serum. *Lane 4*: A reference of D4B5 (Millipore, Bedford, MA), a mouse monoclonal antibody against the γ2 subunit of laminin-332. IgG from patient's serum and D4B5 reacts with the γ2 subunit of laminin-332 (105 kd).

spreading. Although several cases of autoimmune blistering disease with distinct autoantigens have been reported,[3-5] to our knowledge this is the first case report describing a patient with IgG autoantibodies for three different antigens to the basement membrane zone: BP230, laminin γ1 and the γ2 subunit of laminin-332.

Kazuhiro Kikuchi, MD, PhD,[a,b] Ken Natsuga, MD, PhD,[b] Satoru Shinkuma, MD,[b] Wataru Nishie, MD, PhD,[b] Satoshi Kajita, MD, PhD,[c] Hidetsugu Sato, MD, PhD,[a] and Hiroshi Shimizu, MD, PhD[b]

Department of Dermatology, Obihiro Kosei General Hospital, Obihiro[a]; Department of Dermatology, Hokkaido University Graduate School of Medicine, Sapporo[b]; and Takagi Dermatology Clinic, Obihiro,[c] Japan

Funding sources: None.

Conflicts of interest: None declared.

Reprint requests: Ken Natsuga, MD, PhD, Department of Dermatology, Hokkaido University Graduate School of Medicine, N15 W7, Sapporo 060-8638, Japan

E-mail: natsuga@med.hokudai.ac.jp

REFERENCES

1. Yoshida M, Hamada T, Amagai M, Hashimoto K, Uehara R, Yamaguchi K, et al. Enzyme-linked immunosorbent assay using bacterial recombinant proteins of human BP230 as a diagnostic tool for bullous pemphigoid. J Dermatol Sci 2006;41:21-30.
2. Dainichi T, Kurono S, Ohyama B, Ishii N, Sanzen N, Hayashi M, et al. Anti-laminin gamma-1 pemphigoid. Proc Natl Acad Sci U S A 2009;106:2800-5.
3. Izumi R, Fujimoto M, Yazawa N, Nakashima H, Asashima N, Watanabe R, et al. Bullous pemphigoid positive for anti-BP180 and anti-laminin 5 antibodies in a patient with graft-vs-host disease. J Am Acad Dermatol 2007;56:94-7.
4. Shimanovich I, Petersen EE, Weyers W, Sitaru C, Zillikens D. Subepidermal blistering disease with autoantibodies to both the p200 autoantigen and the alpha3 chain of laminin 5. J Am Acad Dermatol 2005;52:90-2.
5. Mitsuya J, Hara H, Ito K, Ishii N, Hashimoto T, Terui T. Metastatic ovarian carcinoma-associated subepidermal blistering disease with autoantibodies to both the p200 dermal antigen and the gamma 2 subunit of laminin 5 showing unusual clinical features. Br J Dermatol 2008;158:1354-7.

doi:10.1016/j.jaad.2010.09.719

Thrombosis-induced ulcerations of the lower legs with coexistent anetoderma due to antithrombin III deficiency

To the Editor: A 54-year-old white man with schizoaffective disorder and insulin-dependent diabetes mellitus presented with a several-month history of nonhealing, painful ulcerations of the lower extremities. On examination, the right lower extremity had a 10- × 6-cm ulcer with irregular borders. Closer observation revealed numerous flesh-colored, atrophic 1- to 2-cm plaques on skin surrounding the ulceration consistent with anetoderma (Fig 1). These lesions were asymptomatic and began concomitantly with ulcer development. Livedo reticularis was not present. Initial evaluation included a biopsy of the ulceration and laboratory investigation for hereditary and acquired hypercoagulable states. Histologic evaluation of the ulceration revealed deep and superficial thromboses with prominent overlying infarct, without evidence of primary vasculitis or pyoderma gangrenosum. Laboratory evaluation for anti-phospholipid antibodies and cryoglobulins were negative; however, anti-thrombin III activity was reduced. Repeat testing revealed below normal antithrombin III activity (mean, 74%; normal, 80%-120%) and reduced antigen level at 19.6% (normal, 22%-36%). A Doppler ultrasound of the lower extremities was negative for deep vein thrombosis.

Fig 1. Lesions of anetoderma surrounding thrombotic-induced ulceration on right leg.

The patient was referred to the hematology service; a trial of coagulation prophylaxis with enoxaparin (Lovenox, Sanofi-Aventis), 40 mg administered subcutaneously twice daily, was performed. This resulted in complete resolution of all skin lesions over several weeks (Fig 2). Several weeks later, the patient presented with recurrence of lower extremity ulcerations. It was discovered that the patient had self-discontinued treatment with enoxaparin because of pain with medication injection as well as cutaneous bleeding and bruising with minimal trauma. Subsequent replacement with fondaparinux (Arixtra, Glasko Smith Kline, Brentford,

Recurrence of Hydroxyurea-induced Leg Ulcer After Discontinuation of Treatment

Kazuhiro Kikuchi[1], Ken Arita[1], Yasuki Tateishi[1], Masahiro Onozawa[2], Masashi Akiyama[1] and Hiroshi Shimizu[1]
Departments of [1]Dermatology and [2]Hematology, Hokkaido University Graduate School of Medicine, North 15 West 7, Kita-ku, Sapporo 060-8638, Japan.
E-mail: kikku@med.hokudai.ac.jp
Accepted November 1, 2010.

Hydroxyurea (HU) is a hydroxylated derivative of urea that has been recognized since 1960 as effective against cancer (1). It is an inhibitor of cellular DNA synthesis, and it promotes cell death in the S phase of the cell cycle through inhibition of the enzyme ribonucleotide reductase (2). The most common indications for HU therapy are chronic myeloid leukaemia and other myeloproliferative disorders (3, 4) such as essential thrombocythemia (5) and polycythemia vera (PV) (6). Cutaneous side-effects, such as alopecia, diffuse hyperpigmentation, scaling, lichen planus-like lesions, poikiloderma, atrophy of the skin and subcutaneous tissues, and nail changes, can occur during the treatment with HU (7–9). The occurrence of painful leg ulcers represents another rare and incompletely characterized complication that has been described in patients with myeloproliferative diseases receiving high-dose long-term HU treatment (10). While the mode of action of HU on bone marrow elements is well established, its effects on actively proliferating epithelial cells remain less described (11). Poor response to traditional local and systemic therapy is a typical feature of HU-induced leg ulcers, and discontinuation of the drug is often required to achieve complete wound healing (6, 8). Cessation of the drug usually improves the skin ulcer; although, in some cases, the ulcer remains and additional therapies, such as skin grafting, are needed (12). We report here the first case of a leg ulcer that recurred even after discontinuation of HU treatment.

CASE REPORT

The patient was an 82-year-old Japanese male who had been diagnosed with PV 9 years before and had been treated only with phlebotomy and an anti-platelet agent for several years. Due to splenomegaly and elevated blood cell counts, HU therapy was started 3 years ago at a dosage of 1 g daily for a month, followed by 1.0 or 1.5 g daily for 28 months. A good clinical response was achieved. However, the patient developed painful ulcers on the left second toe after two years of HU treatment.

He visited our outpatient clinic and was diagnosed with an HU-induced skin ulcer. HU was discontinued, topical application of sulfadiazine silver was performed, an oral antibiotic (cefdinir) was administered, and the ulcer epithelialized. However, a new ulcer appeared on the left lateral malleolar area 46 days after cessation of HU and gradually enlarged in size. The patient was admitted to our hospital for treatment of the ulcer.

Examination revealed a 48 × 56 mm ulcer with yellow necrotic tissue and marginal erythematous oedema (Fig. 1). Laboratory examination revealed a white blood cell count of $11.6 \times 10^3/\mu l$, a platelet count of $64.2 \times 10^4/l$, and a red blood cell count of $5.07 \times 10^6/\mu l$. Anti-nuclear antibody, anti-neutrophilic cytoplasmic antibodies, anti-cardiolipin antibody, and cryoglobulin were negative. A skin biopsy taken from the margin of the ulcer demonstrated leukocytoclastic vasculitis in the upper dermis (Fig. 2). A wound-healing strategy of surgical debridement, intravenous prostaglandin E1 administration, and topical application of beta-fibroblast growth factor, sulfadiazine silver and alprostadil alfadex was started, and the ulcer began to epithelialize. After 4 months, re-epithelialization was complete. The PV was treated with busulfan, achieving a good clinical response.

DISCUSSION

HU is usually well tolerated and has low toxicity (1). However, cutaneous adverse effects such as diffuse hyperpigmentation, brown discoloration of the nails, acral erythema, photosensitization, fixed drug eruption, alopecia, and oral ulceration have been reported (7–9). Stahl & Silber (10) first reported HU-induced skin ulcers in 1985. Montefusco et al. (11) reported

Fig. 1. Left foot with an ulcer on the lateral malleolar area after two months free of hydroxyurea administration. The ulcer was covered with yellow necrotic tissue and surrounded by oedematous erythema.

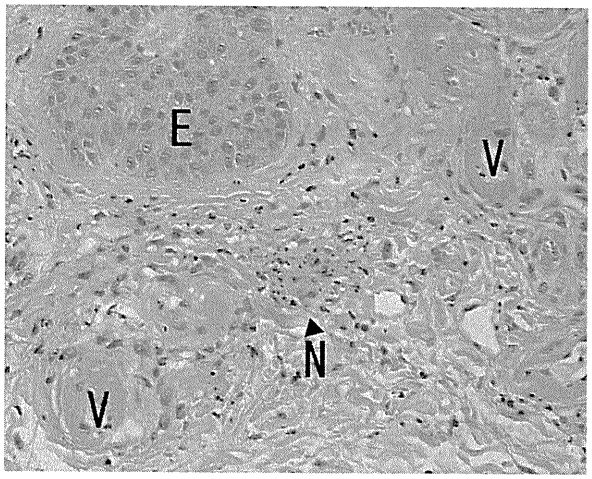

Fig. 2. Histology of erythema on the margin of the ulcer (haematoxylin-eosin staining). Fibrin deposition on the vascular wall and nucleic debris were evident around small vessels (×100). (E: epidermis; V: blood vessels; N: neutrophilic nuclear debris).

that, among 200 chronic myeloid leukaemia patients treated with HU, 17 (8.5%) developed leg ulcers. However, they achieved complete resolution or significant improvement after discontinuation of HU therapy (11). HU-induced leg ulcer and complete resolution within several months after drug discontinuation has also been reported in other myeloproliferative disorder, such as PV (6) and essential thrombocythemia (5). In those cases, as in ours, most of the patients had been treated with > 1 g of HU per day for at least one year (8). In the present case, the patient was treated with > 1 g of HU per day for 28 months. The ulcer occurred on his lateral malleolus, which histologically showed leukocytoclastic vasculitis. These features are consistent with previous reports of HU-induced leg ulcer.

From previous reports, the pathogenesis of HU-induced ulceration remains unclear and it may be multifactorial. It has been postulated that ulcers may be the result of: (*i*) interruption of microcirculation due to leukocytoclastic vasculitis or arterial microthrombi related to platelet dysregulation (13, 14); (*ii*) cumulative toxicity in the basal layer of the epidermis through inhibition of DNA synthesis (8); and (*iii*) repeated mechanical injury in areas subject to trauma: a perimalleolar area for instance (15).

In the case described here, a new ulcer developed even after cessation of HU administration. As for the pathogenic mechanism of recurrence, (*i*) interruption of microcirculation could result from hyperviscosity due to the elevated platelet count (as high as 100×10^4/l in one measurement) (13, 14), although no thrombi were observed histologically in the capillaries or small vessels. (*ii*) The direct cytotoxic effect of HU (8) may continue even after the withdrawal of the drug, and it may inhibit the repair of (*iii*) small injuries in the perimalleolar area: the one of the area susceptible to physical trauma (15). These assumptions can be made from the pathogenesis of HU-induced ulcer reported previously (8, 13–15).

To our knowledge, this is the first report of recurrence of HU-related leg ulcer after the discontinuation of medication. The case suggests that it is important to pay careful attention to recurrence even after cessation of HU therapy. Precise, early treatment for microtraumas and small ulcers should be administered to patients with a long history of HU medication.

REFERENCES

1. Boyd AS, Neldner KH. Hydroxyurea therapy. J Am Acad Dermatol 1991; 25: 518–524.
2. Yarbro JW. Mechanism of action of hydroxyurea. Semin Oncol 1992; 19: 1–10.
3. Goldman JM. Therapeutic strategies for chronic myeloid leukemia in the chronic (stable) phase. Semin Hematol 2003; 40: 10–17.
4. Rice L, Baker KR. Current management of the myeloproliferative disorders: a case-based review. Arch Pathol Lab Med 2006; 130: 1151–1156.
5. Demirçay Z, Cömert A, Adigüzel C. Leg ulcers and hydroxyurea: report of three cases with essential thrombocythemia. Int J Dermatol 2002; 41: 872–874.
6. Bader U, Banyai M, Böni R, Burg G, Hafner J. Leg ulcers in patients with myeloproliferative disorders: disease- or treatment-related? Dermatology 2000; 200: 45–48.
7. Najean Y, Rain JD. Treatment of polycythemia vera: the use of hydroxyurea and pipobroman in 292 patients under the age of 65 years. Blood 1997; 90: 3370–3377.
8. Weinlich G, Schuler G, Greil R, Kofler H, Fritsch P. Leg ulcers associated with long-term hydroxyurea therapy. J Am Acad Dermatol 1998; 39: 372–374.
9. Daoud MS, Gibson LE, Pittelkow MR. Hydroxyurea dermopathy: a unique lichenoid eruption complicating long-term therapy with hydroxyurea. J Am Acad Dermatol 1997; 36: 178–182.
10. Stahl RL, Silber R. Vasculitic leg ulcers in chronic myelogenous leukemia. Am J Hematol 1985; 78: 869–872.
11. Montefusco E, Alimena G, Gastaldi R, Carlesimo OA, Valesini G, Mandelli F. Unusual dermatologic toxicity of long-term therapy with hydroxyurea in chronic myelogenous leukaemia. Tumori 1986; 72: 317–321.
12. Kato N, Kimura K, Yasukawa K, Yoshida K. Hydroxyurea-related leg ulcers in a patient with chronic myelogenous leukemia: a case report and review of the literature. J Dermatol 1999; 26: 56–62.
13. Sirieix ME, Debure C, Baudot N, Dubertret L, Roux ME, Morel P, et al. Leg ulcers and hydroxyurea: forty-one cases. Arch Dermatol 1999; 135: 818–820.
14. Chaine B, Neonato MG, Girot R, Aractingi S. Cutaneous adverse reactions to hydroxyurea in patients with sickle cell disease. Arch Dermatol 2001; 137: 467–470.
15. Saravu K, Velappan P, Lakshmi N, Shastry BA, Thomas J. Hydroxyurea induced perimalleolar ulcers. J Korean Med Sci 2006; 21: 177–179.

Case Reports in Dermatology

Case Rep Dermatol 2011;3:181–185
DOI: 10.1159/000331325

Published online:
August 26, 2011

ISSN 1662–6567
www.karger.com/cde

Spontaneous Remission of Solitary-Type Infantile Myofibromatosis

Kazuhiro Kikuchi[a] Riichiro Abe[a] Satoru Shinkuma[a]
Erika Hamasaka[a] Ken Natsuga[a] Hiroo Hata[a]
Yasuki Tateishi[a] Masahiko Shibata[a] Yuki Tomita[a]
Yukiko Abe[a] Satoru Aoyagi[a] Makio Mukai[b]
Hiroshi Shimizu[a]

[a]Department of Dermatology, Hokkaido University Graduate School of Medicine, Sapporo, and [b]Department of Pathology, Keio University School of Medicine, Tokyo, Japan

Key Words
Infantile myofibromatosis · Leiomyosarcoma · Solitary type

Abstract
Infantile myofibromatosis is a rare fibrous tumor of infancy. The cutaneous solitary type has typically an excellent prognosis. However, histologically, it is important to rule out leiomyosarcoma, which has a poor prognosis. The low frequency of mitosis was definitive for a diagnosis of infantile myofibromatosis. We present a cutaneous solitary-type case of infantile myofibromatosis. Following incisional biopsy, the tumor remitted spontaneously.

Introduction

Infantile myofibromatosis is a benign fibrous tumor of infancy and was first described by Stout in 1954 [1]. In most cases, it is present at birth, and in 90% of cases, the tumor appears within the first 2 years of life [2, 3]. The prognosis is excellent in the solitary type, which is limited in the skin, muscle, and subcutaneous lesions [2–4]. In contrast, the multicentric form of infantile myofibromatosis, which has visceral involvement, can be life-threatening [4, 5]. The solitary type is usually benign and the recurrence rate is low at 10%. Therefore, surgical excision is recommended [2, 6].

Kazuhiro Kikuchi, MD, PhD

Department of Dermatology
Hokkaido University Graduate School of Medicine, N15 W7, Kita-ku
Sapporo 060-8638 (Japan)
Tel. +81 11 716 1161, E-Mail kikku@med.hokudai.ac.jp

Case Rep Dermatol 2011;3:181–185
DOI: 10.1159/000331325
Published online: August 26, 2011

ISSN 1662–6567
www.karger.com/cde

We present a case of a 3-week-old girl showing features of infantile myofibromatosis (solitary type). Excision was performed and no recurrence was detected in 24 months' follow-up.

Case Report

A 3-week-old, otherwise healthy Japanese girl had a solid, red-colored, cutaneous nodule on left shoulder. The nodule had a central concavity with a crust on the surface and measured 20 × 21 mm in diameter (fig. 1).

Physical examination and CT imaging of the head, chest, abdomen and pelvis revealed no additional lesions. No infiltration of the tumor into the muscle was identified by MRI imaging (fig. 2). Incisional biopsy was performed when the patient was 4 months old. The specimen showed multifocal sclerotic dermal nodules. The nodules were composed of spindle cells with round or oval nuclei and eosinophilic cytoplasm. Delicate bundles of eosinophilic fibers separated the cellular aggregates (fig. 3a, b). A diagnosis of infantile myofibromatosis, leiomyoma, leiomyosarcoma, histiocytoma, or other sarcoma was suggested. Spindle cells expressed smooth muscle actin (fig. 3c), but not caldesmon, desmin or S100 protein (not shown). The mitotic figures were very infrequent [6 mitoses per 10 low-power images (40×)]. These results were confirmed to be consistent with infantile myofibromatosis. The tumor gradually regressed until it completely disappeared 24 months after biopsy.

Discussion

Infantile myofibromatosis usually develops at birth or during the first years of life. Chung and Enzinger found the median age at presentation to be 3 months [2]. A slight male predominance among patients with both the solitary and multicentric variants was noted by Wiswell et al. [7]. Most cases of infantile myofibromatosis are solitary nodules, accounting for up to 70% of cases in one study [2], and up to 80% in another series [4]. The prognosis is excellent in the solitary type [2–4]. In the case of solitary-type infantile myofibromatosis, spontaneous regression can be expected [3, 4]. In contrast, a quarter of the cases with the multicentric form may have visceral involvement and can be life-threatening [2, 4, 5]. The solitary type of infantile myofibromatosis is usually benign and is typically found in the dermis, subcutis, or deep soft tissues. The distribution is predominantly on the head, neck, and trunk like our case. Involvement of the extremities is reported to be rare [2]. Solitary infantile myofibromatosis on an upper extremity accounted for only 13.3% in one study of 45 cases [8].

The histologic hallmark of infantile myofibromatosis is an un-encapsulated, well-circumscribed lobule of peripheral spindle cells, which bear a close resemblance to smooth muscle [9, 10]. Often there is a central area of hemangiopericytoma-like small rounded cells surrounding blood vessels [11, 12]. This combination of features gives infantile myofibromatosis its recognizable biphasic appearance, though the hemangiopericytoma-like appearance was not detected in this case. The presence of smooth muscle actin in the spindle cells indicates the diagnosis of infantile myofibromatosis or leiomyosarcoma. Considering the difference in prognosis, it was necessary to rule out leiomyosarcoma [13] in this case. While at least 1 mitotic cell per field in high-power (×200 or ×400) fields is detected in leiomyosarcoma [14], very infrequent mitotic figures [6 mitotic cells per 10 low-power (×40) fields] were observed, which definitively indicated infantile myofibromatosis in this case.

Case Rep Dermatol 2011;3:181–185
DOI: 10.1159/000331325
Published online: August 26, 2011

ISSN 1662–6567
www.karger.com/cde

Previously, radical excision had been advocated as the treatment of choice, because it had been believed that the solitary form gave rise to multiple nodules with potential visceral involvement by metastases [15]. However, it is now more probable that the solitary and multicentric forms are distinct entities and that the solitary form remains localized and can regress [15]. Therefore, a wait-and-see approach has been suggested more recently as a treatment option [15]. However, in our patient, the decision was ultimately made to treat with surgical removal to exclude a diagnosis of leiomyosarcoma, which would have had a poor prognosis. The nodule disappeared completely after excision. The course was consistent with previous reports of solitary-type infantile myofibromatosis [2, 4, 15], and supports our histological diagnosis.

Fig. 1. Solid, red-colored subcutaneous nodule with a central concavity on the left shoulder.

Case Rep Dermatol 2011;3:181–185
DOI: 10.1159/000331325
Published online: August 26, 2011

ISSN 1662–6567
www.karger.com/cde

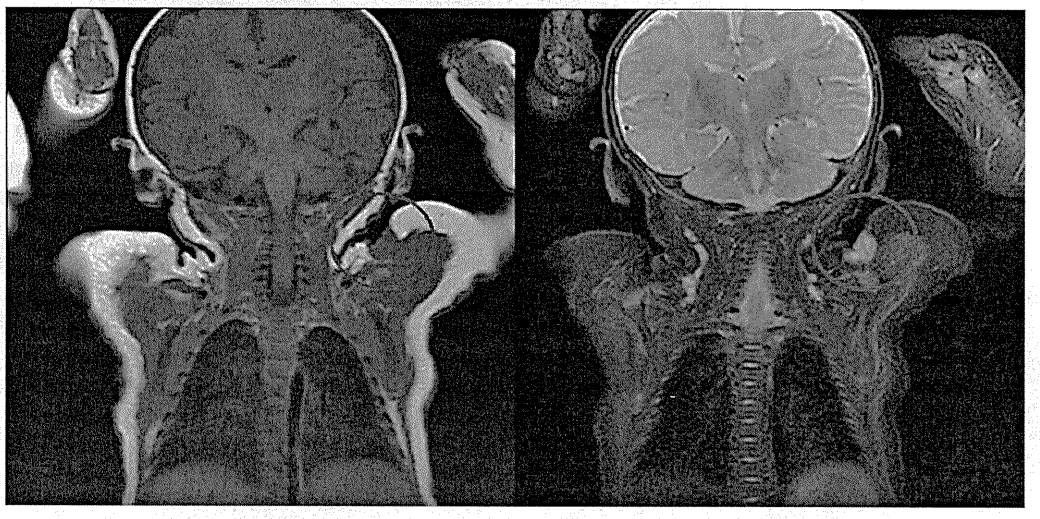

Fig. 2. MRI imaging showed the intensity of the nodule was similar to that of muscle. No additional lesions were found and infiltration of the tumor into the muscle was not observed.

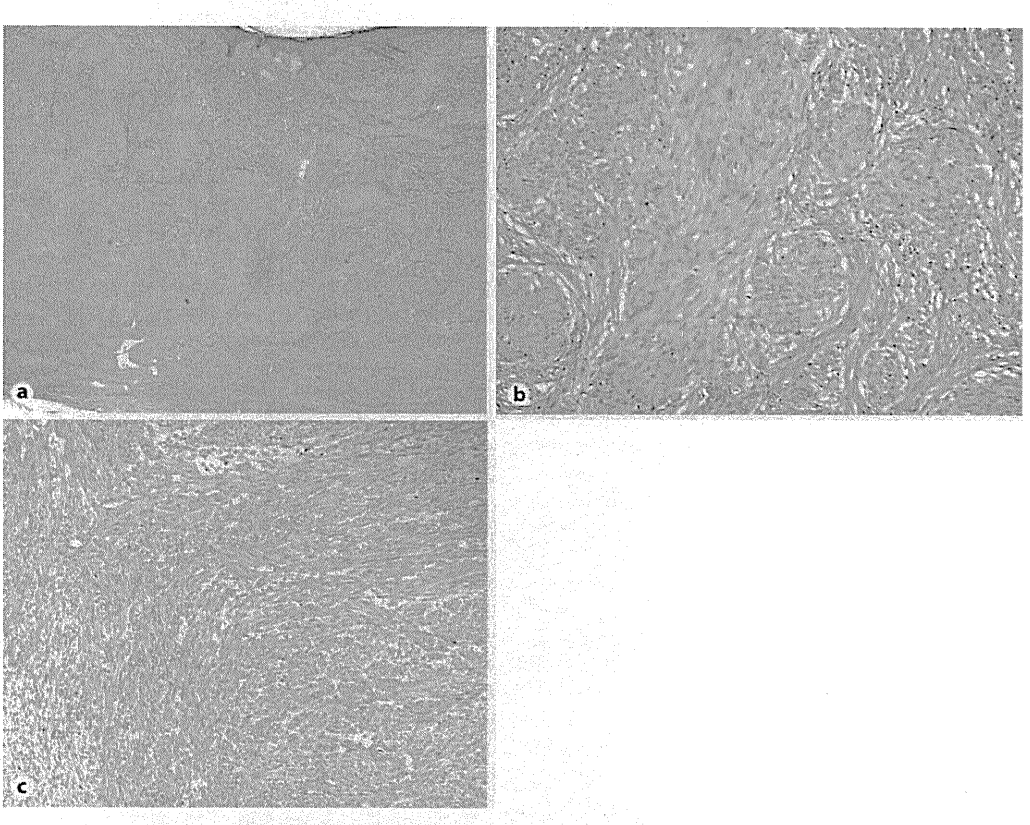

Fig. 3. Hematoxylin-eosin stain, original magnification ×20 (**a**), and ×100 (**b**). Specimen showed multifocal sclerotic dermal nodules composed of spindle cells and eosinophilic fibers. **c** Immunological staining of the tumor for α-smooth muscle actin (×100). Spindle cells express smooth muscle actin.

Case Rep Dermatol 2011;3:181–185
DOI: 10.1159/000331325
Published online: August 26, 2011

ISSN 1662–6567
www.karger.com/cde

References

1 Stout AP: Juvenile fibromatosis. Cancer 1954;7:953–978.

2 Chung EB, Enzinger FM: Infantile myofibromatosis. Cancer 1981;48:1807–1818.

3 Larralde M, Hoffner MV, Boggio P, Abad ME, Luna PC, Correa N: Infantile myofibromatosis: report of nine patients. Pediatr Dermatol 2010;27:29–33.

4 Stanford D, Rogers M: Dermatological presentations of infantile myofibromatosis: a review of 27 cases. Australas J Dermatol 2000;41:156–161.

5 Goldberg NS, Bauer BS, Kraus H, Crussi FG, Esterly NB: Infantile myofibromatosis: a review of clinicopathology with perspectives on new treatment choices. Pediatr Dermatol 1988;5:37–46.

6 Hogan SF, Salassa JR: Recurrent adult myofibromatosis: a case report. Am J Clin Pathol 1992;97:810–814.

7 Wiswell TE, Sakas EL, Stephenson SR, Lesica JJ, Reddoch SR: Infantile myofibromatosis. Pediatrics 1985;76:981–984.

8 Ang P, Tay Y, Walford Y: Infantile myofibromatosis: a case report and review of the literature. Cutis 2004;73:229–231.

9 Dictor M, Elner A, Andersson T, Fernö M: Myofibromatosis-like hemangiopericytoma metastasizing as differentiated vascular smooth-muscle and myosarcoma. Am J Surg Pathol 1992;16:1239–1247.

10 Granter SR, Badizadegan K, Fletcher CD: Myofibromatosis in adults, glomangiopericytoma, and myopericytoma: a spectrum of tumors showing perivascular myoid differentiation. Am J Surg Pathol 1998;22:513–525.

11 Weedon D: Tumors and tumor-like proliferations; in Weedon D (ed): Skin Pathology, ed 2. Philadelphia, Churchill Livingstone, 2002, pp 767–768.

12 Variend S, Bax NMA, van Gorp J: Are infantile myofibromatosis, congenital fibrosarcoma and congenital hemangiopericytoma histogenetically related? Histopathology 1995;26:57–62.

13 Fields JP, Helwig EB: Leiomyosarcoma of the skin and subcutaneous tissue. Cancer 1981;47:156–169.

14 Staut AP, Hill WT: Leiomyosarcoma of the superficial soft tissues. Cancer 1958;11:844–854.

15 Toren A, Perlman M, Polak-Charcon S, Avigad I, Katz M, Kuint Y, Rechavi G: Congenital hemangiopericytoma/infantile myofibromatosis: radical surgery versus a conservative 'wait and see' approach. Pediatr Hematol Oncol 1997;14:387–393.

Biomaterials 32 (2011) 4782–4792

Contents lists available at ScienceDirect

Biomaterials

journal homepage: www.elsevier.com/locate/biomaterials

A denatured collagen microfiber scaffold seeded with human fibroblasts and keratinocytes for skin grafting

Margit Kempf [a,1], Yuki Miyamura [b,1], Pei-Yun Liu [a], Alice C.-H. Chen [a], Hideki Nakamura [b], Hiroshi Shimizu [b], Yasuhiko Tabata [c], Roy M. Kimble [a], James R. McMillan [a,b,*,1]

[a] Centre for Children's Burns and Trauma Research (CCBTR), The University of Queensland, Queensland Children's Medical Research Institute, Brisbane, Australia
[b] Department of Dermatology, Hokkaido University Graduate School of Medicine, Sapporo, Japan
[c] Department of Biomaterials, Field of Tissue Engineering, Institute for Frontier Medical Sciences, Kyoto University, Japan

ARTICLE INFO

Article history:
Received 31 January 2011
Accepted 9 March 2011
Available online 8 April 2011

Keywords:
Collagen
Dermis
Scaffold
Keratinocyte
Fibroblast
Surface graft

ABSTRACT

Biomaterial scaffolds are categorized into artificial or natural polymers, or combinations of the two. Artificial polymers often undergo serum protein adsorption, elicit foreign body and encapsulation immune responses post-implantation. Large pore bovine electrospun collagen I was therefore screened as a candidate for human keratinocyte and fibroblast cell scaffolds. Human HaCaT keratinocyte and dermal fibroblasts were seeded on electrospun denatured collagen I microfiber (DCM) scaffolds and after 72 h Livedead® assays performed to determine adhesive cell, survival and scaffold penetration. Both keratinocytes and fibroblasts attached to and survived on DCM scaffolds, however only fibroblasts migrated over and into this biomaterial. HaCaT keratinocytes remained largely stationary on the scaffold surface in discrete islands of monolayered cells. For this reason, normal human epidermal keratinocyte (NHEK) scaffold interactions were assessed using scanning and transmission electron microscopy (EM) that demonstrated DCM scaffolds comprised networks of interlocking and protruding collagen fibers with a mean diameter of 2–5 μm, with a mean inter-fiber pore size of 6.7 μm (range 3–10 μm) and scaffold thickness 50–70 μm. After 72 h the keratinocytes and fibroblasts on DCM scaffolds had attached, flattened and spread over the entire scaffold with assembly of lamellapodia and focal adhesion (FA)-like junctions. Using transmission EM, NHEKs and HaCaT keratinocytes assembled desmosomes, lamellapodia and FA junctions, however, neither hemidesmosomes nor basal lamina were present. In long term (21 day) co-culture fibroblasts migrated throughout the scaffold and primary keratinocytes (and to a lesser extend HaCaTs) stratified on the scaffold surface forming a human skin equivalent (HSE). *In vivo* testing of these HSEs on immunocompetent (BalbC) and immunodeficient (SCID) excisionally wounded model mice demonstrated scaffold wound biocompatibility and ability to deliver human cells after scaffold biodegradation.

1. Introduction

Skin tissue engineering addresses the need for early, permanent coverage of extensive skin injury in burns patients with an insufficient source of autologous skin for grafting [1,2]. Severe burn injuries require prompt wound closure but are hampered by limited patient donor site area and the high number of separate surgical operations often required to complete treatment [1,2]. In clinical situations in which insufficient donor skin is available, bioengineered skin in the form of cultured keratinocytes or in combination with fibroblasts to form human skin equivalents (HSEs) has allowed a greater expansion of donor surface area than conventional methods [3]. Cultured skin keratinocyte sheets are typically too fragile for transfer *in vitro* for engraftment and are commonly supported by biomaterial scaffolds that mimic specific tissues [4,5]. Such biomimetic scaffolds are classified into either naturally occurring [6–8] or artificial substrates [9] or combinations of the two source materials. We have previously tested artificial polymers that have many favorable properties [9], although

Abbreviations: DCM, Denatured collagen microfiber; NHEK, Normal human epidermal keratinocytes.

* Corresponding author. Centre Children's for Burns and Trauma Research, (CCBTR), Queensland Children's Medical Research Institute (QCMRI), L/4 RCH Foundation Building, Royal Children's Hospital, Herston, Brisbane, QLD 4029, Australia. Tel.: +61 (0) 7 3636 9069; fax: +61 (0) 7 3365 5455.
E-mail address: j.mcmillan@uq.edu.au (J.R. McMillan).

[1] These authors contributed equally to this paper.

0142-9612/$ – see front matter © 2011 Elsevier Ltd. All rights reserved.
doi:10.1016/j.biomaterials.2011.03.023

unfortunately some polymers have generally not performed up to expectations in the clinical setting [10–11]. Here, we examine the efficacy of a natural polymer scaffold derived from bovine collagen I. Previous biomimetic scaffolds have included freeze dried collagen sponges alone [4], sponges seeded with fibroblasts [12], collagen I scaffolds cross-linked with elastin [13], collagen II scaffolds [14], collagen and artificial polymer mixes [15–17], collagen cross-linked by carbodiimide [18] or electrospun collagen alone [19–21], electrospun collagen with epidermal keratinocytes [22] and scaffolds co-cultured with fibroblasts and keratinocytes [8,23]. The advantages of electrospun denatured collagen microfiber (DCM) scaffolds over frozen sponges come from a more homogenous pore structure and closer biomimetic structure to naturally occurring extracellular matrix [23] with pores of 5–10 microns allowing penetration of fibroblasts into the scaffold [24].

An important function of any potential skin substitute is to support the formation of a proper epidermal barrier to limit transepidermal water loss, infection and reduce the chances of hypertrophic scarring by speeding wound closure and ultimately patient recovery [25]. While the need to replace the epidermal barrier is paramount, restoration of normal structure and function of dermal tissue architecture is also critical to achieve acceptable cosmetic results [25]. Currently, there are very few skin substitutes that meet all of these criteria; however, recent cultured skin substitutes comprising fibroblast and keratinocyte cells on natural scaffolds meet many graft requirements [3,23]. The use of natural scaffolds patterned in novel ways to support reconstituted HSEs has primarily focused on reducing scar formation in animal wound models [8]. There are currently several animal wound models on which to test engraftment of human bioengineered skin composites onto immunodeficient mice to assess scarring [26]. In this study we have evaluated the use of DCM scaffold for supporting different human keratinocyte and fibroblast cell combinations for the preparation and transplantation of skin grafts from *in vitro* cultures. We have used *in vitro* cell viability assays to assess HaCaT keratinocyte and fibroblast cell attachment, survival, migration and morphology on DCM scaffolds. Due to the limitations of HaCaT cells to stratify in culture we also included primary human keratinocyte containing cultures in ultrastructural and functional HSE grafts studies. The biocompatibility of the DCM scaffold without cells was tested in excisionally wounded immunocompetent mice. In addition, the efficacy of different cell combinations of DCM composite grafts were tested in excisionally wounded immunocompromised SCID mice. Furthermore, the ability of the grafts to deliver live human cells and improve specific wound healing outcomes including reducing wound closure rates, shortening re-epithelialization times, reducing dermal foreign body and encapsulation immune responses and reducing dermal fibrosis was also assessed.

2. Materials and methods

2.1. Preparation of biomaterial

Denatured collagen microfiber (DCM) scaffolds were manufactured as previously described using acid extraction techniques [18] and subsequently disinfected/sterilized (using ethanol and UV light sterilization), washed, air dried and vacuum stored until required. Fiber diameter and morphology of the electrospun scaffold were controlled by concentration and molecular weight of the polymer as previously described [21,24,27]. Fiber diameters of 3–10 μm (greater than 3–4 μm) were produced to allow fibroblast cells to migrate into the scaffold [9]. Upon cell inoculation trapped air was removed using a combination of serial ethanol and sterile 0.1M Dulbecco's phosphate buffered saline (PBS) washes. This biomaterial was submersed in DMEM medium (Invitrogen, Gibco, BRL, Carlsbad CA, USA) before seeded with cultures of human fibroblasts or keratinocytes (HaCaT) keratinocyte cell line or primary normal human epidermal keratinocytes (NHEKs) or in combination. Sterilized, dehydrated DCM biomaterial was directly used for immunocompetent BalbC mouse biocompatibility experiments.

2.2. Cell sources

The cells (keratinocytes or fibroblasts) were only seeded on the upper DCM biomaterial surface. Fibroblast cells were sustained in Dulbecco's Modified Eagles Medium (DMEM) medium with 10% Fetal Calf Serum (FCS), penicillin and streptomycin (Gibco/Invitrogen, Mulgrave, Vic, Australia). HaCaT cells a gift from Dr. N. Fusening (German Cancer Research Center, Heidelberg, Germany) [28] were also maintained in DMEM medium (Gibco/Invitrogen, Mulgrave, Vic, Australia). Normal human neonatal foreskin keratinocytes (Cambrex, Walkersville, MD, catalogue number CC-2503) were grown or isolated in KGM I culture medium (Clonetics, MD/Cambrex, Walkersville, MD, USA) until passage 2 or 3 (P2/P3). Alternatively, primary keratinocytes obtained from surgical specimens (with institutional ethical approval) were maintained in SFM medium (Gibco/Invitrogen, Mulgrave, Vic, Australia) and supplemented with EGF and BPE growth factor supplements (as per the manufacturer's instructions). The cells were then trypsinized and stored in 10% DMSO under liquid nitrogen until required. Normal human dermal fibroblasts were obtained from surgical specimens or commercially (Cambrex, Walkersville, MD, catalogue number 1/2F0-C25) and grown in DMEM with 10% FCS (Cambrex, Walkersville, MD) until passage 5 (P5). Cells were then trypsinized and stored in 10% DMSO under liquid nitrogen until required.

To create primary keratinocyte-fibroblast composites that have the ability to form a stratified epidermis in culture, $1 \times 10^5/cm^2$ fibroblasts were seeded onto a DMEM medium pre-soaked DCM scaffold at day 0 (seeded cells were maintained in place on the DCM by a modified pipette tip used as an insert). From day 1 these cells were maintained in UCMC 160 medium [29] as previously described [23]. Concurrent with fibroblast confluence on the DCM on day 5, $1 \times 10^6/cm^2$ keratinocytes were directly seeded in UCMC 160 medium onto the scaffold composites to create a bilayered composite (again, using the modified pipette tip as a retainer). At day 6 the insert was removed and the composite was placed into 6 well plates and transferred onto a nylon mesh platform (Mersilene™ Polyester Fiber Mesh, Ethicon, Johnson and Johnson, Langhorne, PA) to maintain it at the air–liquid interface. From day 10 onwards neither progesterone nor EGF growth factors (supplied with UCMC 160 medium) were added to the UCMC 160 medium. Composites were maintained in UCMC 160 until day 26 with a culture medium change at least every 48 h.

2.3. Livedead® cell survival assay

Low passage, HaCaT keratinocytes (<P10) or dermal fibroblasts (<P5) were expanded and maintained in the previously described DMEM culture medium. Cells were trypsinized, counted and 3.5×10^5 cells per cm^2 plated onto pre-prepared DCM substrate. This density has previously been determined to be sufficient for proper seeding of keratinocytes onto grafts [9,30]. Cells were stringently washed 4 times in sterile 0.1M Dulbecco's phosphate buffered saline to removed non-adherent cells and maintained for 72 h on DCM biomaterial. After 72 h, the cell-biomaterial composites were then subjected to the Livedead® fluorescence assay according to the manufacturer's instructions and the numbers of live (green) non-viable/dead (red) cells (either HaCaT keratinocytes or fibroblasts) immediately assessed using an Olympus Fluoview FV300 confocal and IX70 inverted microscope (Olympus, Tokyo, Japan) with a ×20 objective lens. Only attached, live, uniformly green fluorescent cells or typically small, pyknotic red cells were counted. The mean percentage of live (green florescent) and pyknotic red (dead) cells were calculated (from $n = 3$ microscope fields of view repeated three times) as a fraction of total cell numbers represented by the presence of counterstained cell nuclei. Statistical analysis was performed between identical control cells grown on tissue culture plastic (TCP) the treatment groups using one way analysis of variance and two sample *t*-tests using the Minitab statistical package (Minitab Incorporated, University of Pennsylvania, Philadelphia, PA, USA) at a p value <0.05 or <0.01 showing significant effects.

2.4. Scanning electron microscopy

DCM substrate alone or monocultures of cells on DCM substrate (fibroblasts, HaCaTs or primary keratinocyte) were maintained for 72 h and subsequently fixed in 2% glutaraldehyde for at least 4 h and processed for routine scanning electron microscopy (SEM) as previously described [9]. Briefly, samples were dehydrated in a graded ethanol series, treated twice with isoamyl acetate, critical point CO_2 dried using a Hitachi HCP-2 (Hitachi, Tokyo, Japan) followed by optional platinum-palladium sputter coating in a Hitachi E–1030 (Hitachi, Tokyo, Japan). Specimens were examined using either a Hitachi S-4500 or JEOL 6400F SEM microscope fitted with a digital image capture system (Japan Electron Optical Ltd, Tokyo, Japan). Over 100 surface adherent cells were examined as a representative sample per cell type on the DCM substrate.

2.5. Transmission electron microscopy

Cell monocultures (keratinocytes or fibroblasts) were maintained on films for over 72 h (between 3 and 26 days) and were fixed in 2% glutaraldehyde solution, post-fixed in 1% OsO_4, dehydrated, and processed for conventional electron microscopic observation according to the methods described by [9]. Semithin sections were cut and stained with Richardson's stain and mounted using cyanoacrylate glue [31,32].